SLAC-PUB-9532
October 2002

Radiative Corrections to Fixed Target Møller Scattering Including Hard Bremsstrahlung Effects *

Frank J. Petriello

Stanford Linear Accelerator Center

Stanford University

Stanford CA 94309, USA

Abstract

We present a calculation of the complete $\mathcal{O}(\alpha)$ electroweak radiative corrections to the Møller scattering process $e^-e^- \to e^-e^-$, including hard bremsstrahlung contributions. We study the effects of these corrections on both the total cross section and polarization asymmetry measured in low energy fixed target experiments. Numerical results are presented for the experimental cuts relevant for E-158, a fixed target e^-e^- experiment being performed at SLAC; the effect of hard bremsstrahlung is to shift the measured polarization asymmetry by $\approx +4\%$. We briefly discuss the remaining theoretical uncertainty in the prediction for the low energy Møller scattering polarization asymmetry.

*Work supported by the Department of Energy, Contract DE-AC03-76SF00515

1 Introduction

The search for physics beyond the Standard Model (SM) can be pursued in two distinct ways: by observing the direct production of particles associated with this new physics, or by detecting the indirect influence of these new states on precision measurements. Since the discovery of the top quark in the early 1990s, no new elementary particle has been found. However, many indirect constraints on the SM and its possible extensions have been obtained by experiment. For example, high precision measurements on the Z-pole at LEP, combined with the values of M_W and m_t measured at the Tevatron, have constrained the mass of the SM Higgs boson to satisfy the bound $m_H < 196$ GeV at 95% CL by studying its influence on the radiative corrections to $Z \to f\bar{f}$ decays [1]. Similarly, the parameter space available to supersymmetric theories is becoming restricted by the absence of CP-violating electric dipole moments which are required in supersymmetric models to explain the baryon asymmetry of the universe via electroweak baryogenesis [2, 3].

There are currently several quantities whose measured values do not match their SM predictions. The value of the muon $g-2$ [4], $\sin^2(\theta_W)$ as derived from the low energy neutrino-nucleon scattering experiment NuTeV [5], and the magnitude of atomic parity violation (APV) in the cesium atom [6] have all been recently reported to deviate from their SM prediction by $\gtrsim 2.5\,\sigma$. The interpretation of these discrepancies, however, is rendered difficult by our current inability to reliably calculate the required hadronic or atomic physics that affects these quantities. The deviations discussed above have been argued to either be less significant or to vanish altogether when the relevant contributions are more carefully analyzed [7].

These results increase the importance of E-158, a fixed target e^-e^- experiment currently being performed at SLAC [8]. This experiment will determine $\sin^2(\theta_W)$ at a momentum transfer $Q^2 \approx 0.02\,\mathrm{GeV}^2$, comparable to the value relevant for neutrino-nucleon scattering, by measuring the polarization asymmetry $A_{LR} = (\sigma_L - \sigma_R)/(\sigma_L + \sigma_R)$ in the Møller scattering process $e^-e^- \to e^-e^-$; this reaction is less sensitive to the hadronic physics that complicates the previous measurement of $\sin^2(\theta_W)$ by NuTeV, and its interpretation should therefore not be plagued by uncontrollable theoretical uncertainties. The error on the E-158 measurement is expected to reach $\delta A_{LR}/A_{LR} \approx \pm 8\%$, corresponding to $\delta \sin^2(\theta_W) = \pm 0.0008$, making it the most accurate determination of $\sin^2(\theta_W)$ at low

momentum transfer [9].

The study of the electroweak (EW) radiative corrections to Møller scattering was initiated by Czarnecki and Marciano [10]. They found that the one-loop corrections reduce the tree-level prediction for A_{LR} by $\approx 40\%$ at low Q^2 in a $\overline{MS}$ renormalization scheme; the large size of this effect can be traced to the fact that while the tree level prediction is proportional to the numerically small electron vector coupling, $g_v = -1/4 + \sin^2(\theta_W) \approx -10^{-2}$, the one-loop result contains quark contributions to $\gamma - Z$ mixing not similarly suppressed. Although the light quark components cannot be computed in perturbation theory, they can be related to $e^+e^- \to$ hadrons scattering data; the analysis of [10] concludes that these effects can be determined with adequate precision. The virtual electroweak corrections to Møller scattering for arbitrary energies were calculated in [11], while the pure QED component of $e^-e^- \to e^-e^-$ was computed in [12] without experimental cuts. Neither of these results is sufficient for comparison with the E-158 measurement.

In this paper we compute the complete $\mathcal{O}(\alpha)$ EW corrections to Møller scattering, including hard bremsstrahlung effects, and impose the experimental cuts relevant for the E-158 measurement at SLAC. Our recalculation of the virtual EW corrections is valid for arbitrary center-of-mass energies and serves as a check of the results in [11], with which we agree. We find that the majority of the QED corrections to A_{LR} cancel when both virtual and hard photon corrections are added, as anticipated in [10, 11]; they contribute only a small $\approx +4\%$ shift to A_{LR}. This is due to the experimental setup of E-158, which treats photons inclusively.

The paper is organized as follows. In Section 2 we present our notation and briefly discuss the tree-level Møller scattering process. We describe the calculation of the one-loop electroweak corrections in Section 3, and explain the treatment of the hard bremsstrahlung effects in Section 4. We present the appropriate experimental cuts and numerical results in Section 5, and conclude in Section 6.

2 Preliminaries and leading order results

In this section we present the Born-level predictions for the unpolarized cross section and polarization asymmetry for the process $e^-(p_1)e^-(p_2) \to e^-(q_1)e^-(q_2)$. The notation introduced here will be used throughout the paper.

We first introduce the following Mandelstam invariants:

$$
\begin{aligned}
s &= (p_1 + p_2)^2 \ , \qquad s^{'} = (q_1 + q_2)^2 \ , \\
t &= (p_1 - q_1)^2 \ , \qquad t^{'} = (p_2 - q_2)^2 \ , \\
u &= (p_1 - q_2)^2 \ , \qquad u^{'} = (p_2 - q_1)^2 \ .
\end{aligned} \tag{1}
$$

In the $2 \rightarrow 2$ scattering process described by the Born-level prediction and the virtual corrections, the primed invariants are equivalent to their unprimed counterparts: $s = s^{'}$, $t = t^{'}$, and $u = u^{'}$. These relations will not hold when we consider the corrections arising from photon emission. We next introduce the electron vector and axial couplings to the Z boson, $g_v = -1/4 + s_W^2$ and $g_a = 1/4$, where $s_W^2 = \sin^2(\theta_W)$ is defined in the on-shell renormalization scheme: $s_W^2 = 1 - M_W^2/M_Z^2$. It is convenient to define the following energy-dependent effective couplings:

$$
\begin{aligned}
c_{LL}(x) &= e^2 \left\{ \frac{1}{x} + \frac{(g_v - g_a)^2}{s_W^2 c_W^2 (x - M_Z^2)} \right\} \ , \\
c_{RR}(x) &= e^2 \left\{ \frac{1}{x} + \frac{(g_v + g_a)^2}{s_W^2 c_W^2 (x - M_Z^2)} \right\} \ , \\
c_{LR}(x) &= e^2 \left\{ \frac{1}{x} + \frac{(g_v^2 - g_a^2)}{s_W^2 c_W^2 (x - M_Z^2)} \right\} \ ,
\end{aligned} \tag{2}
$$

where $-e$ is the charge of the electron. Using these expressions, we can write the squared tree-level matrix elements as

$$
\begin{aligned}
|\mathcal{M}_{LL}^0|^2 &= 4 \left(c_{LL}(t) + c_{LL}(u) \right)^2 s^2 \ , \\
|\mathcal{M}_{RR}^0|^2 &= 4 \left(c_{RR}(t) + c_{RR}(u) \right)^2 s^2 \ , \\
|\mathcal{M}_{LR}^0|^2 &= |\mathcal{M}_{RL}^0|^2 = 4 \left(c_{LR}(t) \right)^2 u^2 + 4 \left(c_{LR}(u) \right)^2 t^2 \ .
\end{aligned} \tag{3}
$$

The subscripts encode the polarizations of the initial electrons, with L denoting left-handed states and R representing right-handed states. All terms of $\mathcal{O}(m_e^2/x)$, where m_e is the electron mass and x denotes one of the invariants introduced in Eq. 1, have been neglected. This is an excellent approximation in the relativistic limit, and is appropriate for the E-158 experimental setup. We next define polarized differential cross sections,

$$
\frac{d\sigma_{ij}}{d\Omega} = \frac{|\mathcal{M}_{ij}|^2}{128\pi^2 s} \ , \tag{4}
$$

and let σ_{ij} denote the integration of these expressions over the region under consideration. We remind the reader that the cross section is invariant under boosts along the beam axis if the boundaries of integration are chosen consistently in each frame. The unpolarized cross section and polarization asymmetry can now be written as

$$\begin{aligned} \sigma_u &= \frac{1}{4}\left\{\sigma_{LL}+\sigma_{LR}+\sigma_{RL}+\sigma_{RR}\right\} \ , \\ A_{LR} &= \frac{\sigma_{LL}+\sigma_{LR}-\sigma_{RL}-\sigma_{RR}}{\sigma_{LL}+\sigma_{LR}+\sigma_{RL}+\sigma_{RR}} \ . \end{aligned} \tag{5}$$

Before discussing the electroweak corrections to these quantities, we comment briefly on our on-shell choice of s_W^2. Numerically, $s_W^2 \approx 0.2216$ in the on-shell scheme, while the Z-pole value is $s_W^2 \approx 0.2315$. Recalling that the tree-level A_{LR} is proportional to $g_v = -1/4 + \sin^2(\theta_W)$, we see that the choice of the on-shell renormalization scheme tends to increase the tree-level asymmetry; the value of A_{LR} is also affected by our choice of M_W as an input, rather than G_μ as in [10]. We will find that the electroweak corrections to the Born-level prediction are larger in the on-shell scheme than in the $\overline{MS}$ scheme chosen in [10]. This indicates that the prescription of [10] is probably a more appropriate parameterization of the tree-level prediction; however, since we will primarily study the effects of hard bremsstrahlung on A_{LR}, this fact will not concern us here.

3 Virtual corrections

In this section we study the one-loop electroweak corrections to the Møller scattering process. We reduce all one-loop integrals to the scalar Passarino-Veltman basis [13] using FORM [14]; the numerical evaluation of the resulting integrals is then performed using *LoopTools* [15]. The matrix elements obtained are valid for $\sqrt{s} \gg m_e$. Since the resulting expressions are rather lengthy, and have been previously discussed in the literature [11], we will not present them explicitly in this manuscript; they are available upon request from the author. We use dimensional regularization to regulate ultraviolet divergences, and an anticommuting γ_5; this is appropriate since no ABJ anomalies are present [16].

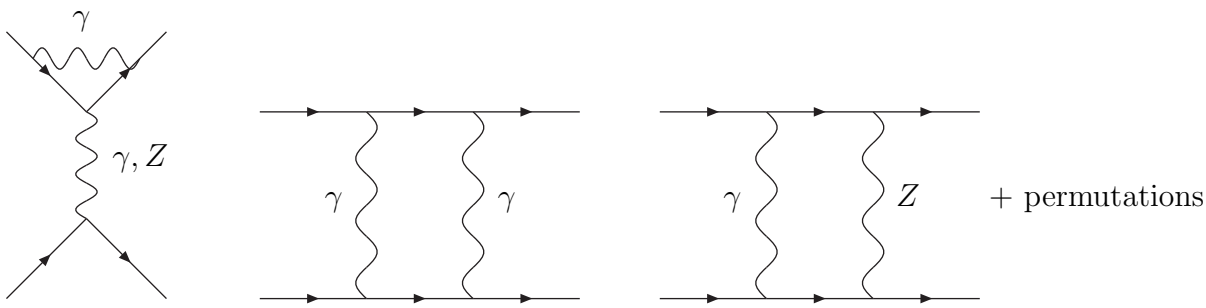

Figure 1: Representative diagrams contributing to the one-loop QED corrections to Møller scattering.

3.1 QED corrections

We follow [11] and define the QED corrections to consist of those diagrams where one photon leg has been attached to a tree-level diagram. A representative sample of the relevant graphs is presented in Fig. 1. We work in the complete on-shell renormalization scheme of [17], in which self-energy corrections to external fermions do not explicitly appear.

These diagrams contain both infrared (IR) and ultraviolet (UV) divergences. We regulate the IR divergences with a finite photon mass μ; these cancel against identical divergences appearing in the process $e^-e^- \to e^-e^-\gamma$, where the photon has an energy $k \leq \Delta E \ll \sqrt{s}$. In this soft photon limit, the integral over the photon phase space factorizes, and its effect is to multiply the tree-level squared matrix elements by the following correction factor Δ_s:

$$|\mathcal{M}^s_{ij}|^2 = \Delta_s \, |\mathcal{M}^0_{ij}|^2 \ , \tag{6}$$

where Δ_s has been derived in [11] and is given by

$$\Delta_s = \frac{\alpha}{\pi} \left\{ 4 \ln\left(\frac{2\Delta E}{\mu}\right) \left[\ln\left(\frac{ut}{m_e^2 s}\right) - 1 \right] - \left[\ln\left(\frac{s}{m_e^2}\right) - 1 \right]^2 + 1 - \frac{\pi^2}{3} + \ln^2\left(\frac{u}{t}\right) \right\} \ . \tag{7}$$

The appearance of the cutoff energy ΔE indicates that this expression is frame-dependent. The E-158 experiment measures the fully inclusive cross section $e^-e^- \to e^-e^- + (n)\gamma$; the dependence on ΔE will therefore cancel from our results when hard bremsstrahlung effects are included, and we need not consider this issue. The UV divergences can be cancelled by the following wavefunction renormalization of the electron field: $\psi_e \to (1 + 1/2\, \delta Z_\psi)\, \psi_e$. This renormalization introduces counterterms for both the $\gamma \bar{f} f$ and $Z \bar{f} f$ vertices. In the

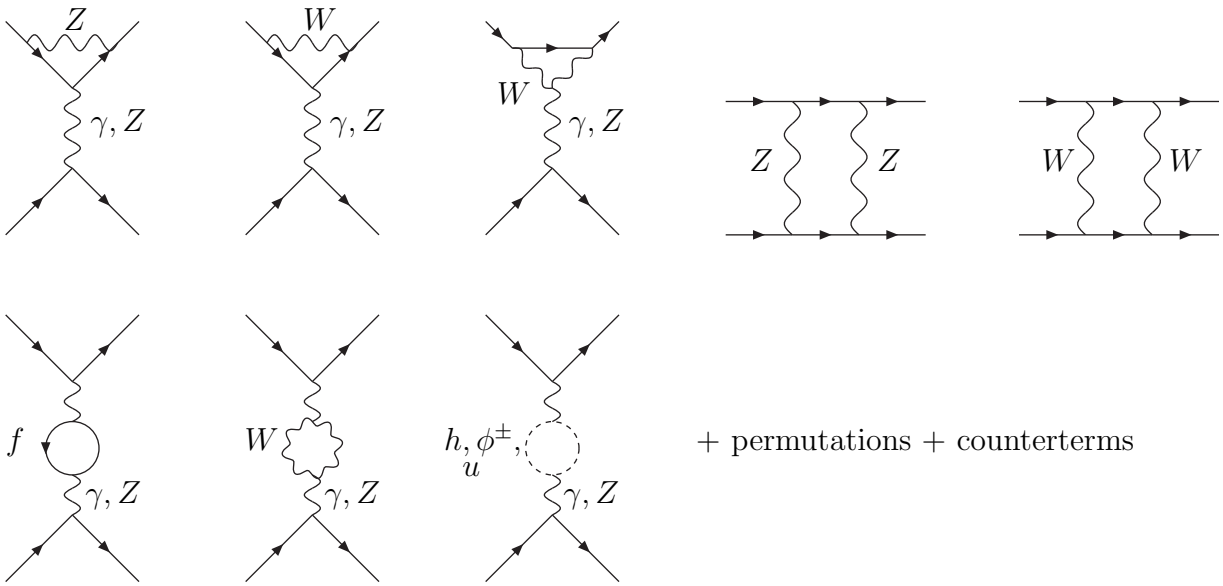

Figure 2: Representative diagrams contributing to the one-loop weak corrections to Møller scattering.

on-shell scheme, δZ_ψ can be written in terms of Passarino-Veltman (PV) functions as

$$\delta Z_\psi = -\frac{\alpha}{4\pi}\left\{B_0\left(0, m_e, 0\right) - 1 - 4m_e^2\, B_0^{'}\left(m_e^2, m_e, \mu\right)\right\} \ , \tag{8}$$

where α is the fine structure constant, B_0 is the two-point PV function in the notation of [17], and $B_0^{'}$ is the derivative of this function with respect to its first argument. $B_0^{'}$ is infrared divergent, and we have therefore retained its dependence on the photon mass μ.

Denoting the one-loop QED matrix elements by $\mathcal{M}_{ij}^Q$, we can write the QED corrections to $|\mathcal{M}_{ij}|^2$ as

$$\delta_{ij}^Q = 2\,\mathrm{Re}\left\{M_{ij}^Q\left(M_{ij}^0\right)^*\right\} + |\mathcal{M}_{ij}^s|^2 \ . \tag{9}$$

3.2 Weak corrections

The one-loop weak corrections to Møller scattering consist of the γ and Z self-energy graphs, $\gamma - Z$ mixing, the remaining vertex and box diagrams, and the appropriate self-energy and vertex counterterms; a representative subset of the countributing graphs is presented in Fig. 2. These contributions contain UV divergences, which must be removed via the full

SM renormalization program; we follow the on-shell prescription described in [17]. The self-energy and counterterm graphs can be combined and interfered with the Born-level diagrams to yield

$$\begin{aligned}
\mathcal{M}^0_{LL}\left(\mathcal{M}^{s+c}_{LL}\right)^* &= 4\,e^2\left(\left\{c_{LL}(t)+c_{LL}(u)\right\}\left\{\mathcal{V}_{LL}(t)+\mathcal{V}_{LL}(u)\right\}\right)s^2\ , \\
\mathcal{M}^0_{RR}\left(\mathcal{M}^{s+c}_{RR}\right)^* &= 4\,e^2\left(\left\{c_{RR}(t)+c_{RR}(u)\right\}\left\{\mathcal{V}_{RR}(t)+\mathcal{V}_{RR}(u)\right\}\right)s^2\ , \\
\mathcal{M}^0_{LR}\left(\mathcal{M}^{s+c}_{LR}\right)^* &= \mathcal{M}^0_{RL}\left(\mathcal{M}^{s+c}_{RL}\right)^* = 4\,e^2\left(c_{LR}(t)\,\mathcal{V}_{LR}(t)\,u^2+c_{LR}(u)\,\mathcal{V}_{LR}(u)\,t^2\right)\ , \qquad (10)
\end{aligned}$$

where the $\mathcal{V}_{ij}(x)$ are given by

$$\begin{aligned}
\mathcal{V}_{LL}(x) &= \left\{2\left(\delta Z_e+\delta Z_L\right)\left[\frac{1}{x}+\frac{g_L^2}{x-M_Z^2}\right]+\frac{g_L}{x-M_Z^2}\,\frac{\delta s_W}{s_W^2c_W^3}+\frac{g_L^2\,\delta M_Z^2}{\left(x-M_Z^2\right)^2}\right. \\
&\quad \left.-\frac{\Sigma^{AA}(x)}{x^2}-2\,\frac{g_L\,\Sigma^{AZ}(x)}{x\left(x-M_Z^2\right)}-\frac{g_L^2\,\Sigma^{ZZ}(x)}{\left(x-M_Z^2\right)^2}\right\}\ , \\
\mathcal{V}_{RR}(x) &= \left\{2\left(\delta Z_e+\delta Z_R\right)\left[\frac{1}{x}+\frac{g_R^2}{x-M_Z^2}\right]+2\,\frac{g_R}{x-M_Z^2}\,\frac{\delta s_W}{c_W^3}+\frac{g_R^2\,\delta M_Z^2}{\left(x-M_Z^2\right)^2}\right. \\
&\quad \left.-\frac{\Sigma^{AA}(x)}{x^2}-2\,\frac{g_R\,\Sigma^{AZ}(x)}{x\left(x-M_Z^2\right)}-\frac{g_R^2\,\Sigma^{ZZ}(x)}{\left(x-M_Z^2\right)^2}\right\}\ , \\
\mathcal{V}_{LR}(x) &= \left\{\left(2\,\delta Z_e+\delta Z_L+\delta Z_R\right)\left[\frac{1}{x}+\frac{g_Lg_R}{x-M_Z^2}\right]+\frac{1}{x-M_Z^2}\left[\frac{g_R}{2\,s_Wc_W}+\frac{g_L\,s_W}{c_W}\right]\frac{\delta s_W}{s_Wc_W^2}\right. \\
&\quad \left.+\frac{g_Lg_R\,\delta M_Z^2}{\left(x-M_Z^2\right)^2}-\frac{\Sigma^{AA}(x)}{x^2}-\frac{\left(g_L+g_R\right)\Sigma^{AZ}(x)}{x\left(x-M_Z^2\right)}-\frac{g_Lg_R\,\Sigma^{ZZ}(x)}{\left(x-M_Z^2\right)^2}\right\}\ . \qquad (11)
\end{aligned}$$

We have introduced the abbreviations $g_L=\left(g_v-g_a\right)/s_Wc_W$ and $g_R=\left(g_v+g_a\right)/s_Wc_W$ for the left and right-handed electron couplings. The forms of the self-energy insertions $\Sigma^{AA}(x)$, $\Sigma^{AZ}(x)$, and $\Sigma^{ZZ}(x)$, as well as expressions for the counterterms δZ_e, δZ_L, δZ_R, δs_W, and δM_Z^2 in terms of these functions, can be found in [17]; note that the pure QED component of Eq. 11 has been considered separately in the previous subsection.

The momentum transfers relevant for the E-158 measurement are $|t|,|u|\approx 0.02\,\mathrm{GeV}^2$. At this energy scale, the light quark contributions to the $\gamma\gamma$ and γZ vacuum polarization functions in Eq. 11 cannot be computed perturbatively; the appropriate degrees of freedom in this regime are the low-lying hadronic states, and the required terms must be obtained by

comparison to experimental data. We discuss here the determination of these contributions. We first consider the expression $2\,\delta Z_e - \Sigma^{AA}(x)/x$. Evaluating the hadronic contributions to this quantity in the free quark approximation, and neglecting the quark masses wherever possible, we find

$$2\,\delta Z_e - \frac{\Sigma^{AA}(x)}{x} = \frac{\alpha}{3\pi}\sum_q Q_q^2 N_c \left\{ \ln\left(\frac{|x|}{m_q^2}\right) - \frac{5}{3} \right\} + \dots \ , \tag{12}$$

where the sum is over the five light quarks and the ellipsis denotes the terms arising from the remaining states. This quantity can be recognized as $\Delta_{\rm had}(x) = \alpha_{\rm had}(0) - \alpha_{\rm had}(x)$, which can be related to $e^+e^- \to$ hadrons scattering data via a dispersion relation [18]. We use the parameterization of $\Delta_{\rm had}(x)$ given in [19], which is a good approximation throughout the entire range of x. A similar calculation reveals that

$$\frac{2\,\delta Z_e}{t - M_Z^2} = \frac{\Delta_{\rm had}(M_Z^2) + \Sigma_q^{AA}(M_Z^2)/M_Z^2}{t - M_Z^2} + \dots \ , \tag{13}$$

where only the light quark components have been explicitly shown; $\Delta_{\rm had}(M_Z^2)$ can again be obtained from [19], while $\Sigma_q^{AA}(M_Z^2)$ can be calculated perturbatively.

Finally, we must discuss the contribution of the $\gamma - Z$ mixing term, $-\Sigma^{AZ}(x)/x\,(x - M_Z^2)$. For $|x|$ much larger than the light quark masses, this quantity can be evaluated perturbatively; as mentioned earlier, this condition does not hold in the E-158 experimental setup. We begin by rewriting this piece using

$$\left[\frac{\Sigma^{AZ}(x)}{x} - \frac{1}{\epsilon}\right] + \frac{1}{\epsilon} = \frac{\Pi_{MS}^{\gamma Z}(x)}{x} + \frac{1}{\epsilon} \ , \tag{14}$$

where $\epsilon = 4 - D$ is the usual regulator appearing in dimensional regularization, and $\Pi_{MS}^{\gamma Z}$ is the γZ vacuum polarization function defined in the $\overline{MS}$ renormalization scheme. The remaining $1/\epsilon$ pole cancels when the counterterms of Eq. 11 are combined with the vertex diagram contributions. We next set $x = 0$ in $\Pi_{MS}^{\gamma Z}$; an estimate of the error induced by evaluating this quantity at $x = 0$ rather than at the value $|x| \approx 0.02\,{\rm GeV}^2$ relevant for the E-158 experiment was performed in [10] by calculating the pion contributions to $\Pi^{\gamma Z}(x)$ in a scalar QED framework. This effect was found to be negligible, and we ignore it in the

remainder of our analysis. Evaluating $\Pi^{\gamma Z}$ in the free quark approximation, we obtain

$$\Pi^{\gamma Z}_{MS}(0) = \frac{\alpha}{2\pi}\sum_q \left\{ N_c Q_q \left[T_3 - 2Q_q s_W^2\right] \left(\frac{1}{3}\ln\left(\frac{m_q^2}{M_Z^2}\right)\right)\right\} \ . \tag{15}$$

A dispersion relation analysis of this quantity was performed in [10, 20]; we use this result and replace

$$\frac{1}{3}\sum_q N_c Q_q \left[T_3 - 2Q_q s_W^2\right] \ln\left(\frac{m_q^2}{M_Z^2}\right) \to -6.88 \pm 0.50 \ . \tag{16}$$

It is claimed in [10] that an improved treatment of the $e^+e^- \to$ hadrons scattering data would reduce the quoted error; an analysis of this type motivated by the needs of a high energy e^-e^- program seems to be underway [21].

Denoting the one-loop weak matrix elements by $\mathcal{M}^W_{ij}$, we can write the weak corrections to $|\mathcal{M}_{ij}|^2$ as

$$\delta^W_{ij} = 2\,\mathrm{Re}\left\{ M^W_{ij}\left(M^0_{ij}\right)^*\right\} \ . \tag{17}$$

The complete one-loop expressions for the matrix elements become

$$|\mathcal{M}_{ij}|^2 = |\mathcal{M}^0_{ij}|^2 + \delta^Q_{ij} + \delta^W_{ij} \ . \tag{18}$$

Our results are in a form valid for all $\sqrt{s} \gg m_e$; we can compare them with the detailed results for the unpolarized cross sections and polarization asymmetries given in Tables 1 and 2 of [11]. When we use the same parameters found there, the older parameterization of $\Delta_{\rm had}(x)$ given in [22], and the light quark masses given in [18], we find complete numerical agreement to the given accuracy.

4 Hard bremsstrahlung corrections

In this section we describe corrections to Møller scattering arising from the process $e^-(p_1)e^-(p_2) \to e^-(q_1)e^-(q_2)\gamma(k)$, in which the emitted photon has an energy $k > \Delta E$. We first discuss the calculation of the relevant matrix elements, and afterwards present our parameterization of the phase space.

In our calculation of the hard bremsstrahlung corrections to Møller scattering, we again work in the relativistic limit $\sqrt{s} \gg m_e$; however, as is well known, m_e cannot be

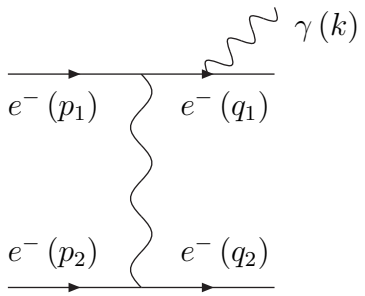

Figure 3: A typical bremsstrahlung diagram; the self-interference of this particular graph neccessitates the inclusion of final-state mass effects.

neglected in regions of the phase space where the emitted photon becomes collinear with one of the electrons. Similarly, m_e must be retained when one of the final-state electrons travels parallel to the beam axis, and the t-channel momentum transfer becomes of $\mathcal{O}\left(m_e^2\right)$. We first perform the calculation neglecting m_e everywhere, and then discuss the required correction factors. We introduce the following abbreviations for the electron propagator denominators connected to an emitted photon:

$$d_1 = \frac{-1}{2p_1 \cdot k}\ , \qquad d_2 = \frac{-1}{2p_2 \cdot k}\ ,$$
$$d_3 = \frac{1}{2q_1 \cdot k}\ , \qquad d_4 = \frac{1}{2q_2 \cdot k}\ . \tag{19}$$

The expressions for the squared matrix elements $|\mathcal{M}_{ij}^{h,a}|^2$ computed with $m_e = 0$ everywhere can be found in Eq. 35 in the Appendix. Recalling the definition of $c_{ij}\left(x\right)$ presented in Eq. 2, we observe that the matrix elements contain peaks of the form s/m_e^2 when one of the following eight quantities becomes of $\mathcal{O}\left(m_e^2\right)$: $1/d_i, t, u, t^{'}, u^{'}$, where $i = 1, 2, 3, 4$. The first four peaking regions are associated with the emitted photon becoming collinear with any of the four electrons, while the remaining four peaks arise when one of the final-state electrons becomes collinear with an initial-state electron. Note that all terms containing $d_i^2, 1/t^2, 1/u^2, 1/t^{'2}$, and $1/u^{'2}$ have cancelled, leaving no contribution which behaves like s^2/m_e^4. However, in the peaking regions, terms of the form $m_e^2 d_i^2$, m_e^2/t^2, etc. are of $\mathcal{O}\left(s/m_e^2\right)$, and must be included; we now discuss the calculation of these pieces.

We first consider the mass effects associated with the unpolarized final-state particles. We focus on $e^-\left(q_1\right)$; the discussion proceeds identically for $e^-\left(q_2\right)$. A typical final-state

bremsstrahlung diagram is shown in Fig. 3; the self-interference of this diagram, or its interference with another diagram where $\gamma(k)$ is emitted from $e^-(q_1)$, leads to the following term in the squared matrix element:

$$\begin{aligned} & \{\not{q}_1 + \not{k} + m_e\} \not{\epsilon}(k)\, u(q_1)\, \bar{u}(q_1)\, \not{\epsilon}^*(k) \{\not{q}_1 + \not{k} + m_e\} (d_3)^2 \\ = \; & \{2q_1 \cdot \epsilon(k) + \not{k}\, \not{\epsilon}(k)\}\, u(q_1)\, \bar{u}(q_1) \{2q_1 \cdot \epsilon^*(k) + \not{k}\, \not{\epsilon}^*(k)\} (d_3)^2 \;, \end{aligned} \tag{20}$$

where $\epsilon(k)$ is the photon polarization vector, $u(q_1)$ is the Dirac spinor of $e^-(q_1)$, and the equality results from the use of the Dirac equation $(\not{q}_1 + m_e)\, u(q_1) = 0$. We now sum over photon polarization vectors and electron spin states; since the electron is unpolarized, we replace $u(q_1)\, \bar{u}(q_1) \rightarrow \not{q}_1 + m_e$. After standard Dirac algebraic manipulations, keeping only $1/d_3$ and $m_e^2/(d_3)^2$ terms, we arrive at the expression

$$2\, \not{q}_1 d_3 - 4\, m_e^2 (\not{k} + \not{q}_1) (d_3)^2 \;. \tag{21}$$

We have obtained the required $1/d_3$ and $m_e^2/(d_3)^2$ terms; the remainder of the numerator algebra can now be performed in the massless limit. We note that d_3 must be evaluated with its full m_e dependence in the peaking region; otherwise, $d_3 \rightarrow \infty$, and an unphysical singularity is encountered.

The calculation of initial-state mass effects is similar to the process outlined above. We find that the squared matrix element contains the term

$$\{2p_1 \cdot \epsilon(k) - \not{k}\, \not{\epsilon}(k)\}\, u(p_1)\, \bar{u}(p_1) \{2p_1 \cdot \epsilon^*(k) - \not{k}\, \not{\epsilon}^*(k)\} (d_1)^2 \tag{22}$$

when self-interference of diagrams with bremsstrahlung off $e^-(p_1)$ is considered; a similar expression is obtained when studying $e^-(p_2)$. Since the initial states can be polarized, we must now replace

$$u(p_1)\, \bar{u}(p_1) \rightarrow \frac{1}{2} (\not{p}_1 + m_e)(1 + \gamma_5\, \not{s}) \;, \tag{23}$$

where

$$\not{s} = P_{||} \left\{ \frac{\not{p}_1}{m_e} - m_e \frac{\not{q}}{p_1 \cdot q} \right\} \;, \tag{24}$$

$P_{||}$ is the degree of longitudinal polarization, and q is an auxiliary vector satisfying $q^2 = 0$, $p_1 \cdot q \neq 0$; for mass effects associated with $e^-(p_1)$, it is convenient to choose $q = p_2$. For the

calculation of mass effects arising from $e^-(p_2)$, we choose $q = p_1$. After performing standard Dirac algebraic manipulations, again keeping only the leading terms which contribute to the squared matrix element, and setting $P_{||} = \pm 1$, we find that Eq. 22 becomes

$$\omega_\pm \left\{ -2 \not{k} d_1 - 4\, m_e^2 \left(\not{p}_1 - \not{k} \right) (d_1)^2 \right\} \mp \frac{4\, m_e^2}{s} \left(\omega_+ - \omega_- \right) \left\{ p_1 \cdot p_2 \not{k} - p_2 \cdot k \left(\not{p}_1 - \not{k} \right) \right\} (d_1)^2 \ , \tag{25}$$

where $\omega_\pm = (1 \pm \gamma_5)/2$ are the spin projection operators. We find a similar expression when calculating the mass effects arising from $e^-(p_2)$. The explicit expressions for the mass correction terms $|\mathcal{M}_{ij}^{h,b}|^2$ can be found in Eq. 36 in the Appendix.

Finally, we must discuss the mass effects which are relevant when $t, u, t^{'}$, or $u^{'}$ becomes of $\mathcal{O}(m_e^2)$. Such terms arise only from photon exchange diagrams, and cancel from the numerator of A_{LR}. We consequently need not worry about any complications arising from polarized initial beams. Eq. 36 already contains terms of the form $m_e^2 c_{ij}^2(x)\, d_k^2 \to m_e^2 d_k^2 / x^2$, which become important when either x or $1/d_k$ is of $\mathcal{O}(m_e^2)$. We need therefore only derive the terms of the form $m_e^2 d_i d_j / x^2$. It is possible to have "overlapping peaks", where both x and $1/d_i$ become of $\mathcal{O}(m_e^2)$ at the same point in phase space. Such events are characterized by a photon traveling in one direction down the beam axis while an electron goes in the opposite direction; momentum conservation then implies that the remaining electron has a very low energy. The experimental cuts relevant for the E-158 measurement require the detection of at least one electron with a reasonably high energy at a large center-of-mass frame angle, thereby eliminating all overlapping peaks. The appropriate mass terms to add to the total unpolarized cross section, $|\mathcal{M}_{\rm unpol}^{h,c}|^2$, can be found in Eq. 37 in the Appendix; the same contribution enters the denominator of A_{LR}.

We now have all of the pieces needed for the hard bremsstrahlung cross section. The matrix elements appearing in the numerator of the polarization asymmetry are

$$|\mathcal{M}_{ij}^{h}|^2 = |\mathcal{M}_{ij}^{h,a}|^2 + |\mathcal{M}_{ij}^{h,b}|^2 \ ; \tag{26}$$

the matrix elements needed for the unpolarized cross section and the asymmetry denominator become

$$|\mathcal{M}_{\rm unpol}^{h}|^2 = \sum_{i,j} \left\{ |\mathcal{M}_{ij}^{h,a}|^2 + |\mathcal{M}_{ij}^{h,b}|^2 \right\} + |\mathcal{M}_{\rm unpol}^{h,c}|^2 \ . \tag{27}$$

We must now present our parameterization of the $e^- e^- \to e^- e^- \gamma$ phase space. We

follow [23] and write the hard bremsstrahlung cross section for a given helicity configuration as

$$\sigma_{ij}^{h} = \frac{1}{4s\,(2\pi)^5} \int ds^{'} \frac{d^3k}{2E_k} \frac{d^3q}{2E_q} \delta^{(4)}\left(p_1 + p_2 - k - q\right) \int \frac{d^3q_1}{2E_1} \frac{d^3q_2}{2E_2} \delta^{(4)}\left(q - q_1 - q_2\right) |\mathcal{M}_{ij}^{h}|^2 \ , \quad (28)$$

where $q = q_1 + q_2$ and the two sets of integrations are separately Lorentz invariant. We choose to evaluate the left set in the center-of-mass (CM) frame, and the right set in the rest frame of the $q_1 + q_2$ system. Doing so, using $s^{'} = (q_1 + q_2)^2 = (p_1 + p_2 - k)^2 = s - 2E_k\sqrt{s}$, and performing an azimuthal integration, we arrive at

$$\sigma_{ij}^{h} = \frac{1}{64s\,(2\pi)^4} \int dE_k\, dc_k\, d\Omega_{12}^{R}\, E_k\, |\mathcal{M}_{ij}^{h}|^2 \ . \quad (29)$$

Ω_{12}^{R} is the rest-frame solid angle of the final-state electron $e^-\left(q_1\right)$; all rest-frame quantities will be denoted by a superscript R, while all lab (fixed target) frame quantities will have a superscript L. Expressions without superscripts, such as the photon energy E_k or the cosine of its production angle $c_k = \cos\left(\theta_k\right)$, denote CM frame quantities. In the absence of experimental cuts, the limits of integration are

$$\Delta E \leq E_k \leq \frac{s - 4\,m_e^2}{2\sqrt{s}} \ , \qquad -1 \leq c_k \leq 1 \ ,$$
$$-1 \leq c_1^R = \cos\left(\theta_1^R\right) \leq 1 \ , \qquad 0 \leq \phi_1^R \leq 2\pi \ . \quad (30)$$

The relevant cuts involve restrictions on the lab frame electron energies and angles; we implement them numerically. It is a simple task to express the Mandelstam invariants of Eq. 1 in terms of these integration variables, and to derive the Lorentz transformations connecting the lab, CM, and rest frames.

The complete expressions for the unpolarized cross section and polarization asymmetry become

$$\begin{aligned} \sigma_u &= \frac{1}{4} \sum_{ij} \left\{ \sigma_{ij} + \sigma_{ij}^{h} \right\} \ , \\ A_{LR} &= \frac{\sigma_{LL} + \sigma_{LL}^{h} + \sigma_{LR} + \sigma_{LR}^{h} - \sigma_{RL} - \sigma_{RL}^{h} - \sigma_{RR} - \sigma_{RR}^{h}}{4\,\sigma_u} \ , \end{aligned} \quad (31)$$

where σ_{ij} is the $2 \to 2$ cross section defined in Eq. 4, and the one-loop matrix elements $|\mathcal{M}_{ij}|^2$ are defined in Eq. 18. We can now study the effects of both virtual and hard bremsstrahlung

corrections on measurements of the total cross section and polarization asymmetry in low energy Møller scattering.

5 Numerical results

In this section we present numerical results for the experimental setup relevant for the E-158 measurement at SLAC. For a detailed description of the E-158 experiment, we refer the reader to [8, 9]; we give below a description of the cuts relevant for our purposes. We remind the reader that we have split the radiative corrections into QED and weak components; we will study the effects of these two types of corrections separately.

We demand that at least one electron be detected, with its lab frame energy and production angle satisfying the following constraints:

$$E^L \geq 10\,\mathrm{GeV}\ , \qquad 4.65\,\mathrm{mrad} \leq \theta^L \leq 8.00\,\mathrm{mrad}\ . \tag{32}$$

The exact form of the angular cut is chosen so that typical scattered electrons have a CM frame angle in the range $-0.5 \lesssim c_1 \lesssim 0$. The structure of the E-158 detector is such that events where both scattered electrons enter the acceptance defined by Eq. 32 are counted twice; with this restriction on θ_1^L, no $2 \to 2$ scattering process leads to such an overcounting. However, events with hard photon emission can create such an effect; we will study their contribution to both the total cross section and A_{LR}. We choose a beam energy $E_b = 48$ GeV, and the following gauge and Higgs boson masses: $M_W = 80.451$ GeV, $M_Z = 91.1875$ GeV, and $m_H = 120$ GeV. We use the fermion masses and fine structure constant given in [24]. With this choice of parameters and cuts, we find the following results for the Born-level and weak-corrected unpolarized cross section and polarization asymmetry:

$$\begin{aligned} \sigma_u^B &= 15.348\,\mu\mathrm{b}\ , \qquad A_{LR}^B = 3.646 \times 10^{-7}\ , \\ \sigma_u^{B+W} &= 15.589\,\mu\mathrm{b}\ , \qquad A_{LR}^{B+W} = 1.756 \times 10^{-7}\ . \end{aligned} \tag{33}$$

The effect of weak radiative corrections is to decrease the polarization asymmetry by $\approx 52\%$. A 48% decrease from weak corrections was found in [11] using the on-shell scheme; this result is for the specific phase space point $c_1 = 0$, different values for M_W, M_Z, and m_H, and an older parameterization of $\Delta\alpha_{\mathrm{had}}$. The two results agree when these differences are taken into account. We will compare our results with the $\overline{MS}$ calculation of [10] after discussing the QED corrections.

We present in Table 1 the QED-corrected cross section and asymmetry, and show the percent shifts from the weak-corrected values σ_u^{B+W} and A_{LR}^{B+W} given in Eq. 33. Both virtual and hard bremsstrahlung corrections are included. In our bremsstrahlung calculation we introduced an energy cutoff ΔE, below which the emitted photon phase space integrals were performed analytically in a soft-photon approximation, and above which the exact bremsstrahlung matrix elements were treated numerically. Since we integrate inclusively over the photon phase space, the dependence on ΔE should cancel; we include in Table 1 our results for four choices of this parameter to verify that this indeed occurs. These results were

ΔE ($\sqrt{s}$)	σ_u (μb)	$\delta^Q \sigma_u$	A_{LR} (10^{-7})	$\delta^Q A_{LR}$
10^{-6}	15.455	-0.86%	1.817	$+3.5\%$
10^{-5}	15.456	-0.85%	1.816	$+3.4\%$
10^{-4}	15.457	-0.85%	1.817	$+3.5\%$
10^{-3}	15.457	-0.85%	1.817	$+3.5\%$

Table 1: Total unpolarized cross section, σ_u, and polarization asymmetry, A_{LR}, for different values of the photon energy cutoff ΔE. Also included are the shifts in these quantities from σ_u^{B+W} and A_{LR}^{B+W}, defined in Eq. 33, induced by QED corrections. ΔE is given in units of $\sqrt{s}$, and σ_u is given in millibarns.

obtained using the Monte Carlo integration program VEGAS [25], with the number of calls to the integrand $N_{call} = 5 \times 10^6$. The statistical error should therefore equal $1/\sqrt{N_{call}} \approx 0.05\%$; we have included enough digits in the values of Table 1 to test this expectation. We see that the variation of σ_u and A_{LR} with ΔE is consistent with this statistical fluctuation. The shift in the total cross section induced by QED corrections is small and negative. The infrared-safe combination of virtual corrections and soft photon emission reduces the cross section, while the hard photon cross section partially compensates. These results are similar to those of [26] for Bhabha scattering, where total QED corrections to the cross section of $\approx -5\%$ were found for $-0.5 \leq c_1 \leq 0$, with an acollinearity cut of 15° on the angle between the final state electron and positron and an energy cut on the detected electrons. Our lack of an acollinearity cut allows kinematical configurations in which an undetected electron travels down the beam axis, and either u, t, u', or t' becomes of $\mathcal{O}(m_e^2)$, adding an additional positive contribution to the QED correction. For illustrative purposes we present the total cross section for three different acollinearity angles in Table 2. The decrease in the cross

section is reduced as the acollinearity angle is increased, and a larger amount of the photon phase space is included.

θ_{acoll}	σ_u (μb)	$\delta^Q \sigma_u$
5°	13.865	-11%
10°	14.407	-7.6%
15°	14.688	-5.8%

Table 2: Total unpolarized cross section, σ_u, for different choices of the acollinearity angle θ_{acoll}. Included are the percent shifts from the weak-corrected value in Eq. 33.

We observe from Table 1 that QED corrections increase the prediction for A_{LR} by $\approx 3.5\%$, leading to a final prediction of $A_{LR} = 1.82 \times 10^{-7}$ in the on-shell scheme. The one-loop $\overline{MS}$ result of [10] is $A_{LR} = (1.80 \pm 0.09 \pm 0.04) \times 10^{-7}$, where the quoted errors arise primarily from the hadronic uncertainties in $\Pi^{\gamma Z}$; this value does not include either bremsstrahlung effects or experimental cuts, and is evaluated at the specific phase space point $\cos(\theta) = 0$ where the tree-level prediction for A_{LR} is maximized. The very close agreement between these results is surprising and to an extent accidental; however, we can identify the following two physics effects which contribute to the agreement: 1) the significant difference between the tree-level prediction for A_{LR} in the on-shell and $\overline{MS}$ renormalization schemes caused by differing choices of $\sin^2(\theta_W)$ is ameliorated once virtual corrections are included, and 2) the experimental cuts relevant for the E-158 measurement render hard bremsstrahlung corrections a small effect. Also, the $\approx +3.5\%$ shift induced by hard photon emission accidentally brings the weak-corrected value of A_{LR} in Eq. 33 into closer agreement with the result of [10]. QED corrections to the photon exchange component of Møller scattering of $\approx 100\%$ are reported in [12]. We believe that the large size of these results arises from the lack of experimental cuts in this calculation; without such restrictions, large contributions from the peaking regions discussed in the previous section greatly enhance the cross section. The effects observed in a realistic experimental setup are significantly smaller, as our calculation demonstrates.

We now briefly review the error on the theoretical prediction for A_{LR}. The uncertainty in the one-loop result arising from hadronic contributions to the γZ vacuum polarization function has been mentioned above and discussed in the previous section; although large,

there is hope that it will be reduced in the future [21]. The remaining errors can be divided into those arising from either higher-order QED or weak corrections. The small magnitude of the QED corrections found in this paper, $\approx 3.5\%$, indicate that the inclusion of $\mathcal{O}(\alpha^2)$ effects are unnecessary; the experimental cuts protect the E-158 measurement from large QED effects. The one-loop weak corrections are large: $\approx 40\%$ in the $\overline{MS}$ scheme and $\approx 50\%$ in the on-shell scheme. However, the size of these effects arises from quark contributions to A_{LR} not suppressed by $1 - 4\sin^2(\theta_W)$, a qualitatively new feature which first appears at $\mathcal{O}(\alpha)$. No similar effect appears at the next order in perturbation theory, and we expect that the higher order corrections are suppressed by a factor of $\alpha/\pi \sim 0.1\%$ relative to the one-loop result[†]. We therefore conclude that the most significant source of theoretical uncertainty on the measurement of A_{LR} arises from the hadronic contributions to the γZ vacuum polarization.

As mentioned above, the E-158 measurement double-counts events where a hard photon knocks both electrons into the detector acceptance; this modifies the prediction for both σ_u and A_{LR}. We find that this leads to the following effective values of the cross section and asymmetry, as well as the following shifts from the weak-corrected results of Eq. 33:

$$\begin{aligned} \sigma_u^{eff} &= 15.613\,\mu\text{b}\ , \qquad \delta^Q_{eff}\sigma_u = +1.5\%\ , \\ A_{LR}^{eff} &= 1.829\times 10^{-7}\ , \qquad \delta^Q_{eff}A_{LR} = +4.2\%\ . \end{aligned} \tag{34}$$

We have chosen $\Delta E = 10^{-4}\sqrt{s}$ to obtain these values, and have checked that the variation with this parameter is consistent with the statistical error of the integration. The overcounting of events leads to an effective increase of the cross section, and increases the shift of A_{LR} to $+4.2\%$; subtracting from this the $\approx 3.5\%$ shift of Table 1, we find that the effect of overcounting is an $\approx +0.7\%$ shift in the measured value of A_{LR}. This effect is small, however, and well within the theoretical error discussed above.

6 Conclusions

We have presented a calculation of the complete $\mathcal{O}(\alpha)$ radiative corrections to Møller scattering, and have discussed their effect on the total cross section and polarization asymmetry

[†]Certain corrections, such as those related the running of α, will induce effects that are suppressed relative to the one-loop result by $\alpha/\pi \ln\left(M_Z^2/m_e^2\right) \approx 5\%$; however, this is still a small shift, and a large class of these contributions can be resummed if better precision is required.

measured in E-158, a low energy fixed target experiment being performed at SLAC. The virtual EW corrections have been previously computed in [11]; our recalculation serves as a check of this result, with which we find complete agreement. Our computation of the hard bremsstrahlung contributions with realistic experimental cuts is the first such result, and provides a complete theoretical prediction for comparison with the E-158 measurement. We find that hard bremsstrahlung effects induce a small $\approx +4\%$ shift in the measured value of A_{LR}; the experimental cuts reduce the sensitivity of both the polarization asymmetry and total cross section to QED corrections.

We have also reviewed the theoretical uncertainty in the prediction for A_{LR}. The largest error arises from hadronic contributions to the γZ vacuum polarization function $\Pi^{\gamma Z}$, as discussed in [10]; an improved dispersion relation analysis of low energy $e^+e^- \to$ hadrons data could reduce this value [21]. Our results indicate that higher order QED corrections are likely to be small in comparison to the error on $\Pi^{\gamma Z}$, and can be safely neglected in the E-158 analysis. The one-loop weak corrections are $\approx 50\%$; although this effect seems dangerously large, it arises from the appearance of effects unsuppressed by the small electron vector coupling, a qualitatively new contribution which first enters at one loop. As no similar effect appears at higher orders, we conclude that the perturbative corrections to A_{LR} are under control.

The results obtained here are applicable to both low energy experiments such as E-158 and future high energy colliders, and provide detailed Standard Model predictions to which measured values can be compared. We hope that they assist in maximizing the discovery potential of both current and future experimental programs.

Acknowledgments

It is a pleasure to thank K. Melnikov for suggesting this project, and for his constant encouragement and assistance. I would also like to thank C. Anastasiou, P. Bosted, L. Dixon, J. Hewett, Y. Kolomensky, T. Rizzo and M. Woods for helpful comments and suggestions. This work was supported in part by the National Science Foundation Graduate Research Program.

Appendix

We collect here the expressions for the various hard bremsstrahlung matrix elements $|\mathcal{M}_{ij}^{h,x}|^2$ discussed in Eqs. 26 and 27. We first consider $|\mathcal{M}_{ij}^{h,a}|^2$, which are computed with $m_e = 0$

everywhere; with the Mandelstam invariants presented in Eq. 1, $c_{ij}(x)$ defined in Eq. 2, and d_i defined in Eq. 19, we can express them as

$$
\begin{aligned}
|\mathcal{M}_{LL}^{h,a}|^2 &= 8e^2 \Big\{ \left(s^2+s^{'2}\right)\left\{t\, c_{LL}^2(t)\, d_2 d_4 + u\, c_{LL}^2(u)\, d_2 d_3 + t^{'} c_{LL}^2(tp)\, d_1 d_3 + u^{'} c_{LL}^2(up)\, d_1 d_4\right\} \\
&\quad -2s^{'}\left\{c_{LL}\left(t^{'}\right) c_{LL}\left(u^{'}\right)\left(s+t^{'}+u^{'}\right) d_1 + c_{LL}(t)\, c_{LL}(u)\,(s+t+u)\, d_2\right\} \\
&\quad -2s\left\{c_{LL}\left(t^{'}\right) c_{LL}(u)\left(s^{'}+t^{'}+u\right) d_3 + c_{LL}(t)\, c_{LL}\left(u^{'}\right)\left(s^{'}+t+u^{'}\right) d_4\right\} \\
&\quad -2\left\{c_{LL}\left(t^{'}\right)+c_{LL}\left(u^{'}\right)\right\}\left\{c_{LL}(t)+c_{LL}(u)\right\} s^{'}\left(t^{'}+u^{'}\right)(t+u)\, d_1 d_2 \\
&\quad -2\left\{c_{LL}\left(t^{'}\right)+c_{LL}(u)\right\}\left\{c_{LL}(t)+c_{LL}\left(u^{'}\right)\right\} s\left(t^{'}+u\right)\left(t+u^{'}\right) d_3 d_4 \\
&\quad -\left\{c_{LL}(u)\, c_{LL}\left(t^{'}\right)+c_{LL}\left(t^{'}\right) c_{LL}\left(u^{'}\right)+c_{LL}(u)\, c_{LL}\left(u^{'}\right)\right\}\left\{tt^{'}\left(s+s^{'}\right)\right. \\
&\quad \left.+ss^{'}\left(t-t^{'}\right)-ss^{'}\left(u+u^{'}\right)-uu^{'}\left(s+s^{'}\right)\right\} d_1 d_3 \\
&\quad -\left\{c_{LL}(t)\, c_{LL}\left(u^{'}\right)+c_{LL}\left(u^{'}\right) c_{LL}\left(t^{'}\right)+c_{LL}(t)\, c_{LL}\left(t^{'}\right)\right\}\left\{uu^{'}\left(s+s^{'}\right)\right. \\
&\quad \left.+ss^{'}\left(u-u^{'}\right)-ss^{'}\left(t+t^{'}\right)-tt^{'}\left(s+s^{'}\right)\right\} d_1 d_4 \\
&\quad -\left\{c_{LL}(u)\, c_{LL}\left(t^{'}\right)+c_{LL}(t)\, c_{LL}(u)+c_{LL}(t)\, c_{LL}\left(t^{'}\right)\right\}\left\{uu^{'}\left(s+s^{'}\right)\right. \\
&\quad \left.+ss^{'}\left(u^{'}-u\right)-ss^{'}\left(t+t^{'}\right)-tt^{'}\left(s+s^{'}\right)\right\} d_2 d_3 \\
&\quad -\left\{c_{LL}(t)\, c_{LL}\left(u^{'}\right)+c_{LL}(u)\, c_{LL}(t)+c_{LL}(u)\, c_{LL}\left(u^{'}\right)\right\}\left\{tt^{'}\left(s+s^{'}\right)\right. \\
&\quad \left.+ss^{'}\left(t^{'}-t\right)-ss^{'}\left(u+u^{'}\right)-uu^{'}\left(s+s^{'}\right)\right\} d_2 d_4 \Big\}\ , \\
|\mathcal{M}_{RR}^{h,a}|^2 &= \left|\mathcal{M}_{LL}^{h,a}\left(c_{LL}(x)\rightarrow c_{RR}(x)\right)\right|^2\ , \\
|\mathcal{M}_{LR}^{h,a}|^2 &= |\mathcal{M}_{RL}^{h,a}|^2 = 8e^2 \Big\{ u\, c_{LR}^2(u)\left(t^2+t^{'2}\right) d_2 d_3 + t\, c_{LR}^2(t)\left(u^2+u^{'2}\right) d_2 d_4 \\
&\quad +t^{'} c_{LR}^2\left(t^{'}\right)\left\{s^2+s^{'2}+t^2-t^{'2}-2t^{'}u-2t^{'}u^{'}+2st+2ss^{'}+2s^{'}t\right\} d_1 d_3 \\
&\quad +u^{'} c_{LR}^2\left(u^{'}\right)\left\{s^2+s^{'2}+u^2-u^{'2}-2u^{'}t-2u^{'}t^{'}+2su+2ss^{'}+2s^{'}u\right\} d_1 d_4 \\
&\quad +\left\{c_{LR}(t)\, c_{LR}\left(t^{'}\right)\left\{\left(u+u^{'}\right)\left(ss^{'}-tt^{'}+uu^{'}\right)+2suu^{'}\right\}\right. \\
&\quad \left.+c_{LR}(u)\, c_{LR}\left(u^{'}\right)\left\{\left(t+t^{'}\right)\left(ss^{'}-uu^{'}+tt^{'}\right)+2stt^{'}\right\}\right\} d_1 d_2 \\
&\quad +\left\{c_{LR}(t)\, c_{LR}\left(t^{'}\right)\left\{\left(u+u^{'}\right)\left(ss^{'}-tt^{'}+uu^{'}\right)+2s^{'}uu^{'}\right\}\right.
\end{aligned}
$$

$$
\begin{aligned}
&+c_{LR}(u)\, c_{LR}\left(u^{'}\right)\left\{\left(t+t^{'}\right)\left(ss^{'}-uu^{'}+tt^{'}\right)+2s^{'}tt^{'}\right\} d_3 d_4 \\
&+2c_{LR}(u)\, c_{LR}\left(u^{'}\right) t^{'}\,(s+u)\left(s^{'}+u^{'}\right) d_1 d_3 \\
&+2c_{LR}(t)\, c_{LR}\left(t^{'}\right) u^{'}\,(s+t)\left(s^{'}+t^{'}\right) d_1 d_4 \\
&+2c_{LR}(t)\, c_{LR}\left(t^{'}\right) u\left(s+t^{'}\right)\left(s^{'}+t\right) d_2 d_3 \\
&+2c_{LR}(u)\, c_{LR}\left(u^{'}\right) t\left(s+u^{'}\right)\left(s^{'}+u\right) d_2 d_4 \Bigg\} \,. \qquad (35)
\end{aligned}
$$

We now present $|\mathcal{M}_{ij}^{h,b}|^2$, the mass terms which become important when $1/d_i \to \mathcal{O}\left(m_e^2\right)$; we find

$$
\begin{aligned}
|\mathcal{M}_{LL}^{h,b}|^2 &= 8e^2\frac{m_e^2}{s}\Bigg\{ -\left\{c_{LL}\left(t^{'}\right)+c_{LL}\left(u^{'}\right)\right\}^2 s^{'}\left\{s^2+\left(t^{'}+u^{'}\right)^2\right\} d_1^2 + c_{LR}^2\left(t^{'}\right) u^{'}\left\{t^{'}\right. \\
&\times(s-u-t)+su+2ss^{'}+s^{'}u^{'}\Big\} d_1^2 + c_{LR}^2\left(u^{'}\right) t^{'}\left\{u^{'}(s-u-t)\right. \\
&+st+2ss^{'}+s^{'}t^{'}\Big\} d_1^2 - \left\{c_{LL}(t)+c_{LL}(u)\right\}^2 s^{'}\left\{s^2+(t+u)^2\right\} d_2^2 \\
&+c_{LR}^2(t)\, u\left\{t\left(s-u^{'}-t^{'}\right)+su^{'}+2ss^{'}+s^{'}u\right\} d_2^2 + c_{LR}^2(u)\, t\left\{u\left(s-u^{'}-t^{'}\right)\right. \\
&+st^{'}+2ss^{'}+s^{'}t\Big\} d_2^2 + 2\left\{c_{LL}(u)+c_{LL}\left(t^{'}\right)\right\}^2 s^2\left(u+t^{'}\right) d_3^2 \\
&+2\left\{c_{LL}(t)+c_{LL}\left(u^{'}\right)\right\}^2 s^2\left(t+u^{'}\right) d_4^2\Bigg\} \,, \\
|\mathcal{M}_{RR}^{h,b}|^2 &= \left|\mathcal{M}_{LL}^{h,b}\left(c_{LL}(x)\to c_{RR}(x)\right)\right|^2 \,, \\
|\mathcal{M}_{LR}^{h,b}|^2 &= 8e^2\frac{m_e^2}{s}\Bigg\{ \left\{c_{RR}\left(t^{'}\right)+c_{RR}\left(u^{'}\right)\right\}^2 s^{'}\left(s+t^{'}+u^{'}\right)^2 d_1^2 - c_{LR}^2\left(t^{'}\right) u^{'} \\
&\times\left\{t^{'}\left(s^{'}+t^{'}+u^{'}\right)+su+s^{'}u^{'}\right\} d_1^2 - c_{LR}^2\left(u^{'}\right) t^{'}\left\{u^{'}\left(s^{'}+t^{'}+u^{'}\right)\right. \\
&+st+s^{'}t^{'}\Big\} d_1^2 + \left\{c_{LL}(t)+c_{LL}(u)\right\}^2 s^{'}(s+t+u)^2 d_2^2 - c_{LR}^2(t)\, u \\
&\times\left\{t\left(s^{'}+t+u\right)+su^{'}+s^{'}u\right\} d_2^2 - c_{LR}^2(u)\, t\left\{u\left(s^{'}+t+u\right)\right. \\
&+st^{'}+s^{'}t\Big\} d_2^2 + 2\, c_{LR}^2(u)\, t^{'}(s+u)\, d_3^2 + 2\, c_{LR}^2\left(t^{'}\right) u\left(s+t^{'}\right) d_3^2 \\
&+2\, c_{LR}^2(t)\, u^{'}(s+t)\, d_4^2 + 2\, c_{LR}^2\left(u^{'}\right) t\left(s+u^{'}\right) d_4^2\Bigg\} \,, \\
|\mathcal{M}_{RL}^{h,b}|^2 &= \left|\mathcal{M}_{LR}^{h,b}\left(c_{LL}(x)\to c_{RR}(x)\right)\right|^2 \,. \qquad (36)
\end{aligned}
$$

Finally, the modification of the total unpolarized cross section that results when $t, u, t^{'}, u^{'} \rightarrow \mathcal{O}\left(m_e^2\right)$ is

$$
\begin{aligned}
|\mathcal{M}_{\text{unpol}}^{h,c}|^2 &= 64\, e^6\, m_e^2 \left\{ \frac{(s+u)\left(s^{'}+u^{'}\right) d_2 d_4}{t^2} + \frac{(s+t)\left(s^{'}+t^{'}\right) d_2 d_3}{u^2} \right. \\
&\left. + \frac{\left(s+u^{'}\right)\left(s^{'}+u\right) d_1 d_3}{t^{'2}} + \frac{\left(s+t^{'}\right)\left(s^{'}+t\right) d_1 d_4}{u^{'2}} \right\} . \qquad (37)
\end{aligned}
$$

References

[1] D. Abbaneo *et al.* [ALEPH Collaboration], arXiv:hep-ex/0112021.

[2] D. Chang, W. F. Chang and W. Y. Keung, arXiv:hep-ph/0205084.

[3] A. Pilaftsis, arXiv:hep-ph/0207277.

[4] G. W. Bennett [Muon g-2 Collaboration], Phys. Rev. Lett. **89**, 101804 (2002) [arXiv:hep-ex/0208001].

[5] G. P. Zeller *et al.* [NuTeV Collaboration], Phys. Rev. Lett. **88**, 091802 (2002) [arXiv:hep-ex/0110059].

[6] S. C. Bennett and C. E. Wieman, Phys. Rev. Lett. **82**, 2484 (1999) [arXiv:hep-ex/9903022].

[7] K. Melnikov, Int. J. Mod. Phys. A **16**, 4591 (2001) [arXiv:hep-ph/0105267]; S. Davidson, S. Forte, P. Gambino, N. Rius and A. Strumia, JHEP **0202**, 037 (2002) [arXiv:hep-ph/0112302]; M. Y. Kuchiev and V. V. Flambaum, arXiv:hep-ph/0206124.

[8] R. Carr *et al.*, SLAC-PROPOSAL-E-158.

[9] Y. Kolomensky, "First results on Møller scattering from E158", talk given at 30th SLAC Summer Institute On Particle Physics: Secrets Of The B Meson (SSI 2002), 5-16 Aug 2002, SLAC, Menlo Park, California.

[10] A. Czarnecki and W. J. Marciano, Phys. Rev. D **53**, 1066 (1996) [arXiv:hep-ph/9507420].

[11] A. Denner and S. Pozzorini, Eur. Phys. J. C **7**, 185 (1999) [arXiv:hep-ph/9807446].

[12] N. M. Shumeiko and J. G. Suarez, J. Phys. G **26**, 113 (2000) [arXiv:hep-ph/9912228].

[13] G. Passarino and M. J. Veltman, Nucl. Phys. B **160**, 151 (1979).

[14] J. A. Vermaseren, arXiv:math-ph/0010025.

[15] T. Hahn and M. Perez-Victoria, Comput. Phys. Commun. **118**, 153 (1999) [arXiv:hep-ph/9807565]; T. Hahn, arXiv:hep-ph/9905354; T. Hahn, Acta Phys. Polon. B **30**, 3469 (1999) [arXiv:hep-ph/9910227].

[16] F. Jegerlehner, Eur. Phys. J. C **18**, 673 (2001) [arXiv:hep-th/0005255].

[17] A. Denner, Fortsch. Phys. **41**, 307 (1993).

[18] F. Jegerlehner, PSI-PR-91-08 *Lectures given at the Theoretical Advanced Study Institute in Elementary Particle Physics, (TASI), Boulder, Colo., Jun 3-29, 1990.*

[19] H. Burkhardt and B. Pietrzyk, Phys. Lett. B **513**, 46 (2001).

[20] W. J. Marciano and A. Sirlin, Phys. Rev. D **29**, 75 (1984) [Erratum-ibid. D **31**, 213 (1985)].

[21] W. Marciano, "Polarized Møller Scattering Asymmetries", talk given at LoopFest: Precision Measurements And Radiative Corrections At A Future Linear Collider, 9-10 May 2002, Upton, New York.

[22] H. Burkhardt and B. Pietrzyk, Phys. Lett. B **356**, 398 (1995).

[23] E. Byckling and K.Kajantie, *Particle Kinematics*, (John Wiley and Sons, London, 1973).

[24] D. E. Groom *et al.* [Particle Data Group Collaboration], Eur. Phys. J. C **15**, 1 (2000).

[25] G. P. Lepage, J. Comput. Phys. **27**, 192 (1978).

[26] F. A. Berends, K. J. Gaemers and R. Gastmans, Nucl. Phys. B **68**, 541 (1974).